USING A STOCHASTIC BACKSCATTER MODEL FOR WALL-MODELLED LARGE EDDY SIMULATION

Johan C. Kok

Royal Netherlands Aerospace Centre NLR

johan.kok@nlr.nl

Abstract

This paper investigates the possibility to extend a hybrid RANS–LES method that employs a stochastic backscatter model to Wall-Modelled LES. The coefficients of the model have been optimized to minimize the log-layer mismatch for channel flow, while maintaining the proper decay rate for isotropic turbulence. Application to the co-flow of a wake and a boundary layer shows that the backscatter model ensures the rapid development of resolved turbulence in stream-wise direction after switching from RANS to LES, both in attached and separated shear layers, without adding synthetic turbulence. An alternative formulation of the backscatter model is also considered that ensures a zero mean value of the stochastic forcing. Results are shown for channel flow and for the co-flow.

1 Introduction

Detached Eddy Simulations (DES) (Spalart, 2009) and similar hybrid RANS–LES methods originally have been conceived to simulate flows with massive separation, which are beyond the reach of RANS. In such simulations, the separated flow is modelled with LES, while the attached boundary layers are modelled with RANS. However, there are also applications without massive flow separation for which RANS does not suffice. For example, the direct computation of broadband noise, such as trailing-edge noise, requires the capturing of resolved turbulence within attached boundary layers. For such applications, a hybrid RANS–LES method should be extended to at least a Wall-Modelled Large Eddy Simulation (WMLES), in which the outer part of the boundary layer is modelled with LES and only the inner part is modelled with RANS.

A well-known problem that occurs when using a hybrid RANS–LES method in WMLES mode is the mismatch of the log layers in the RANS and LES regions. Several approaches have been proposed to tackle this problem, such as IDDES (Shur et al., 2008) and stochastic forcing (Piomelli et al., 2003).

A second problem is the slow development of resolved turbulence when switching from RANS to LES inside an attached boundary layer in stream-wise direction (grey-area issue). Typically, some kind of synthetic turbulence generator is used at this location to accelerate this development (Jarrin et al., 2009). Such approaches, however, may easily introduce strong artificial noise, potentially overwhelming the physical broadband noise.

This paper investigates whether both problems can be addressed by a single method, in particular, a stochastic backscatter model that was developed to mitigate the grey-area issue in separated shear layers for hybrid RANS–LES methods (Kok, 2017).

2 Method

Here, the X-LES method is used (Kok et al., 2004), which is a k–ω based DES method that includes the stochastic backscatter model. The method switches dynamically from RANS to LES when the RANS length scale $l_{\text{RANS}} = \sqrt{k}/\omega$ is larger than the LES length scale $l_{\text{LES}} = C_1\Delta$, with the filter width Δ taken equal to the maximum mesh width of a grid cell. The RANS length scale is then replaced by the LES length scale in the expressions for the eddy viscosity ν_t and for the turbulent dissipation ε. In WMLES mode, the RANS–LES interface is not dynamic, but kept frozen during the simulations at the location where $l_{\text{RANS}} = l_{\text{LES}}$ as determined from the initial RANS solution.

In the LES region, a stochastic source term has been added to the momentum equation that represents the backscatter of energy from subgrid scales to resolved scales, as follows

$$\frac{\partial \rho \boldsymbol{u}}{\partial t} + \ldots = \nabla \times (S_B \boldsymbol{\xi}) \,, \tag{1}$$

with $\boldsymbol{\xi}(\boldsymbol{x}, t)$ a vector of three independent stochastic variables with standard normal distribution and with S_B determining the strength of the forcing, taken proportional to the subgrid kinetic energy k,

$$S_B = C_B \rho k \,, \tag{2}$$

with C_B a model constant. Note that the source term is a divergence-free vector and therefore does not introduce any artificial noise. The stochastic source term is present in the complete LES domain and is correlated both in space and time for mesh widths and time steps smaller than the subgrid scales, with the correlation given by

$$\langle \xi_i(\boldsymbol{x}, t) \xi_j(\boldsymbol{y}, s) \rangle = \delta_{ij} \mathrm{e}^{-d^2/2} \mathrm{e}^{-|t-s|/\tau}, \tag{3}$$

with $d^2 = |\boldsymbol{x}-\boldsymbol{y}|^2/(C_\Delta \Delta^2)$ and $\tau = C_\tau \Delta/\sqrt{k}$. The temporal and spatial correlations are obtained by solving PDEs for the stochastic variables, which are described in detail by Kok (2017).

The coefficients of the X-LES method in WMLES mode, including the stochastic model, were optimized by Henger (2020) for channel flow, minimizing the log-layer mismatch, while maintaining the proper decay rate for isotropic homogeneous turbulence. Essentially, both the strength and the extent of the spatial and temporal correlations of the stochastic source term were increased. This resulted in a higher level of backscatter, which was balanced by an increase of the level of subgrid eddy viscosity to maintain the net decay rate. However, this optimization resulted in a stronger correlation than before between the modelled turbulent kinetic energy k and the stochastic variables $\boldsymbol{\xi}$ in regions of high vorticity. This implies a larger, non-zero mean value of the stochastic source term, constituting a significant artificial contribution to the total Reynolds stress tensor that was not intended. In order to ensure a zero mean value, an alternative formulation of the forcing strength S_B and the subgrid time scale τ is considered here,

$$S_B = C_B \overline{\rho k} \qquad \text{and} \qquad \tau = C_\tau \Delta/\sqrt{\overline{k}} \tag{4}$$

with $\overline{f}$ the running time average of f. A full optimization has not been performed for this alternative formulation, but three different sets of coefficients have been selected from a larger range of test computations. The model coefficients are all given in table 1.

Table 1: X-LES model coefficients

	S_B	C_1	C_B	C_Δ	C_τ
original	(2)	0.08	1.0	0.100	0.050
optimized	(2)	0.12	1.5	0.463	0.231
alternative 1	(4)	0.09	1.3	0.400	0.060
alternative 2	(4)	0.10	1.5	0.450	0.060
alternative 3	(4)	0.12	1.3	0.400	0.140

The flow simulations are performed by NLR's flow solver ENSOLV, which solves the compressible flow equations on multi-block structured grids. It employs a finite-volume method in which the convective terms are discretized by a fourth-order symmetry-preserving scheme with low numerical dispersion and dissipation (Kok, 2009), while the viscous terms are discretized by a standard second-order central scheme. The equations are integrated in time by the second-order backward scheme, typically using a convective CFL in the order of 1/8 to ensure a time-integration error comparable to the spatial-discretization error. Low-Mach pre-conditioning is used for the practically incompressible test cases considered here.

3 Channel flow

As first test case, channel flow at a friction Reynolds number $Re_\tau = u_\tau H/\nu = 1000$ is considered, with u_τ the friction velocity, H the channel half height, and ν the kinematic viscosity. As a reference, the DNS of Lee and Moser (2015) is used, which had a corresponding bulk Reynolds number $Re_b = u_b H/\nu = 20000$ with u_b the bulk velocity. Simulations are performed at a Mach number $M_b = 0.1$ based on the bulk velocity. To drive the flow to the desired friction Reynolds number, a constant body force equal to $\rho u_\tau^2/H$ is added to the x-momentum equation.

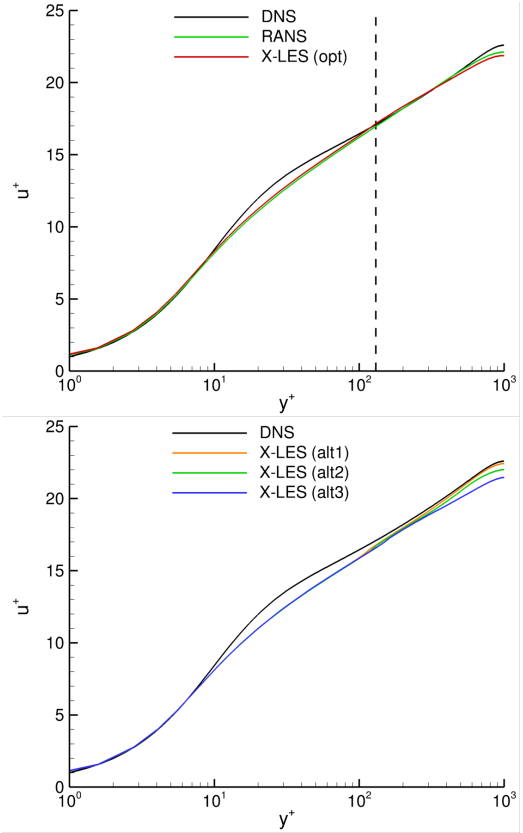

Figure 1: Velocity profiles for channel flow at $Re_\tau = 1000$

The same grid is used as Henger (2020). The domain has a length of $2\pi H$ and a width of πH. The grid has 96 cells in wall-normal direction and is stretched from $\Delta y^+ = 1$ at the wall to $\Delta y^+ = 93$ at the channel centreline using a constant stretching factor. In the other two directions 32 cells are used, giving mesh widths of $\Delta x^+ = 196$ and $\Delta z^+ = 98$. The time step equals $\Delta t = 0.025 H/u_b$ (implying CFL $= u_b \Delta t/\Delta x \approx 1/8$). The simulations are run for 20000 time steps (a time interval of $500 H/u_b$), starting from a RANS solution, and flow statistics are computed over the last 14000 time steps, which was found to be sufficient for statistical convergence.

The computed velocity profiles are shown in figure 1, comparing X-LES in WMLES mode to the reference DNS and RANS (TNT k–ω). The top figure shows the results with the original stochastic source term (using the optimized coefficients of Henger) and the bottom figure with the alternative stochastic term (using the sets of coefficients as defined in table 1). In the top figure, the location of the RANS–LES interface is also indicated by the vertical dashed line (located at

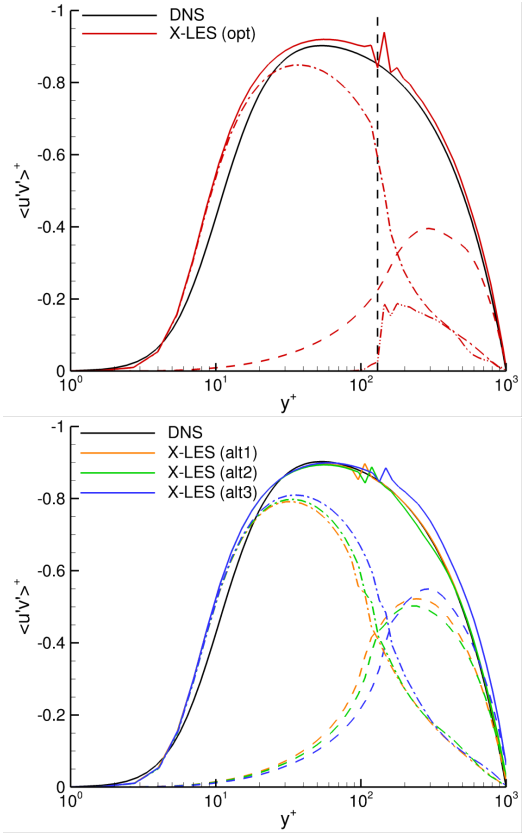

Figure 2: Shear-stress profiles for channel flow at $Re_\tau = 1000$ (solid lines: total stress; dashed lines: resolved stress; dash-dot lines: modelled stress; dash-dot-dot lines: stress due to stochastic term)

$y^+ \approx 130$). No significant log-layer mismatch is discernible in the velocity profiles. The results do show a significant variation of the centreline velocity: alternative 1 gives a velocity closest to the DNS, whereas alternative 3 gives the strongest velocity drop.

Figure 2 shows that the total level of shear stresses in the RANS and LES regions closely match the DNS result, but there is a wiggle visible near the interface. This wiggle may be caused by the stochastic source term being switched on suddenly at the LES side of the interface, but also by freezing the RANS–LES interface at a fixed location, which leads to a slight discontinuity between the RANS and LES length scales at the interface due to the dynamic behaviour of the RANS length scale. For the original stochastic term, an additional non-zero shear stress results from averaging this term and contributes significantly to the total shear stress in the LES region. Using the alternative stochastic term removes this additional non-zero stress. It also results in higher levels of resolved stresses in the LES region and reduces the wiggle.

Finally, the three normal stresses are compared to the DNS in figure 3. Clearly, the results strongly deviate from the DNS in the RANS regions, as may be expected from a standard two-equation turbulence model. At the RANS–LES interface, the modelled stresses rapidly drop and the total stresses tend more

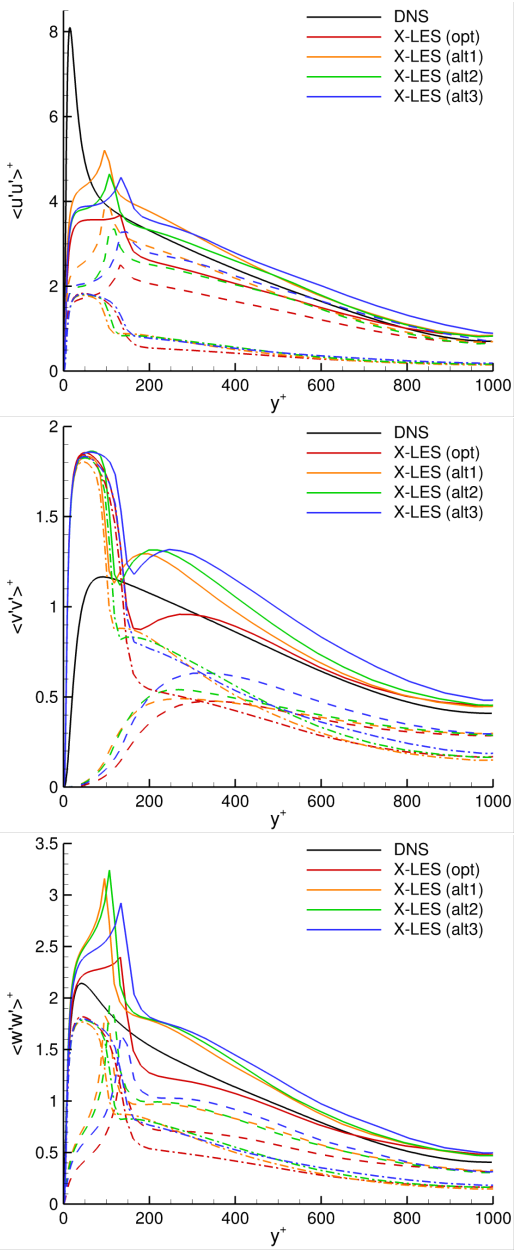

Figure 3: Normal-stress profiles for channel flow at $Re_\tau = 1000$ (solid lines: total stress; dashed lines: resolved stress; dash-dot lines: modelled stress)

to the DNS values. Towards the centre of the channel, generally all WMLES results start to approach the DNS results more closely.

4 Co-flow

In order to test how well the model mitigates the grey-area issue in attached and separated shear layers, the co-flow of a wake and a boundary layer is considered, as defined as test case in the Garteur Action Group 54 (Peng et al., 2020). This case is in particular relevant for high-lift aircraft configurations with deployed flaps and slats, where the wake from the slat will mix with the main wing boundary layer. The set-up follows the experiment of Pot (1979) and consists of two parallel flat plates with a gap between them of

height $h = 35$ mm. The upper plate has a length of $L = 0.5$ m and its wake mixes with the boundary layer on the lower plate which extends downstream for more than 2.5 m. The Reynolds number equals $Re_L = 1.19 \cdot 10^6$ based on the far-field velocity u_∞ and the length L. For the simulations, a far-field Mach number $M_\infty = 0.2$ was used.

An impression of the geometry and near-field grid is given in figure 4. The far-field boundary is located at least 2 m from the upper plate trailing edge, which is located at $x = 0$. The target LES region extends 1.5 m downstream from the upper plate (i.e., from $x = 0$ to $x = 1.5$ m). In this region, a grid has been generated with a target mesh width of 2 mm, both in stream-wise and span-wise directions (corresponding to $\Delta x^+ \approx 200$), while downstream of this region the grid is gradually stretched towards the outflow boundary. A span-wise extent of 0.15 m is used with 72 cells. The wall-normal mesh width equals 0.02 mm at the wall ($\Delta y^+ \approx 2$). In total, the grid consists of 10.45 million cells. The time step equals $\Delta t = 5{\cdot}10^{-4} L/u_\infty$, so that CFL $= u_\infty \Delta t/\Delta x = 1/8$ in the target LES region. Simulations have been performed for 18000 time steps (a time interval of $9L/u_\infty$), gathering flow statistics over the last 8000 steps.

X-LES in WMLES mode is applied in the target LES region and in the region immediately downstream. Outside this region, RANS is applied. Inside the WMLES region, the RANS–LES interface is kept frozen at the location where $l_{\text{RANS}} = l_{\text{LES}}$. Effectively, the RANS layer along the lower plate has a height of $y^+ \approx 150$ up to $x = 1.5$ m, while it grows larger and finally disappears further downstream due to the grid stretching. There is also a small RANS layer around the trailing edge of the upper plate. Note that at the upstream boundary of the WMLES region, no synthetic turbulence is added to the flow to speed-up the development of resolved turbulence. Instead, the computations rely on the stochastic backscatter model.

An instantaneous impression of the flow in the WMLES region, computed using the original stochastic source term, is shown in figures 5 and 6 in terms of the vorticity magnitude and iso-contours of the Q-criterion. Qualitatively, the flows computed using the alternative stochastic terms look very similar (not shown). The boundary layer and wake develop separately up to about $x = 0.5$ to 0.6 m, after which they start to mix. Clearly, resolved turbulence rapidly develops, both in the wake and in the boundary layer, with 3D disturbances visible immediately aft of $x = 0$. This is in stark contrast to DES-type computations (including X-LES and IDDES) without any synthetic turbulence or stochastic forcing for which the development of 3D turbulence is strongly delayed, with typically the flow remaining practically stable in the first half of the LES target region and developing essentially 2D span-wise vortices beyond that (Peng et al., 2020).

Figure 7 shows the mean velocity profiles at six stream-wise stations, with the first five within the target LES region, ranging from $x = 0.008$ m just aft of the upper plate to $x = 1.122$ m, and the last one in the stretched-grid region where the RANS layer has started to grow ($x = 1.722$ m). The velocity profiles closely match the experiment in the wake and in the outer part of the boundary layer, in particular for alternatives 2 and 3. With the original stochastic term, the initial turbulent mixing may be too high, leading to a stronger diffusion of the wake and the outer boundary layer (see station $x = 0.372$ m). The opposite can be said about alternative 1, showing a weaker diffusion of the wake and outer boundary layer (see stations $x = 0.12$ and 0.372 m). In the inner boundary layer, the original formulation shows the closest correspondence to the experiment. The alternative results initially lag behind, with the deficit gradually diminishing and eventually catching up. Note that the experimental results show a deviation from the log law close to the wall, where the measurement accuracy may be reduced.

The shear stresses are compared to the experiment at the same six stations in figure 8. The top figure shows the total shear stress, whereas the bottom one shows the separate components (resolved, modelled, and stochastic) for the original formulation. At the first two stations, the original formulation gives the highest level of total shear stress, close to the RANS solution, but above the experiment, whereas alternative 1 gives the lowest level. This is consistent with the stronger respectively weaker diffusion of the wake and outer boundary layer as observed for the velocity profiles. Further downstream the WMLES results tend to approach each other and the RANS results, in particular at station $x = 1.122$ m, although all results lie slightly above the experiment in the boundary layer and the RANS level is too low at the upper side of the wake. Looking at the separate components, the modelled and stochastic terms are dominant at the first station. At the second station, resolved stresses have already become the largest contribution. At stations three to five, a highly resolved LES is obtained in the wake and outer boundary layer, with the modelled and stochastic terms being negligible there. They only become significant when approaching the RANS wall layer and the modelled stresses become dominant inside the RANS layer. At the last station, the modelling has reverted back to RANS in most of the boundary layer (up to $y/h \approx 0.2$ to 0.3, depending on the value of C_1), with alternative 1 showing the smoothest distribution closest to RANS.

Finally, The skin-friction coefficient for the lower plate is shown in figure 9. There is no experimental data available, therefore only a comparison with RANS can be made. Immediately after switching to WMLES at $x = 0$, there is only a slight drop in skin friction for the original stochastic term, a stronger drop

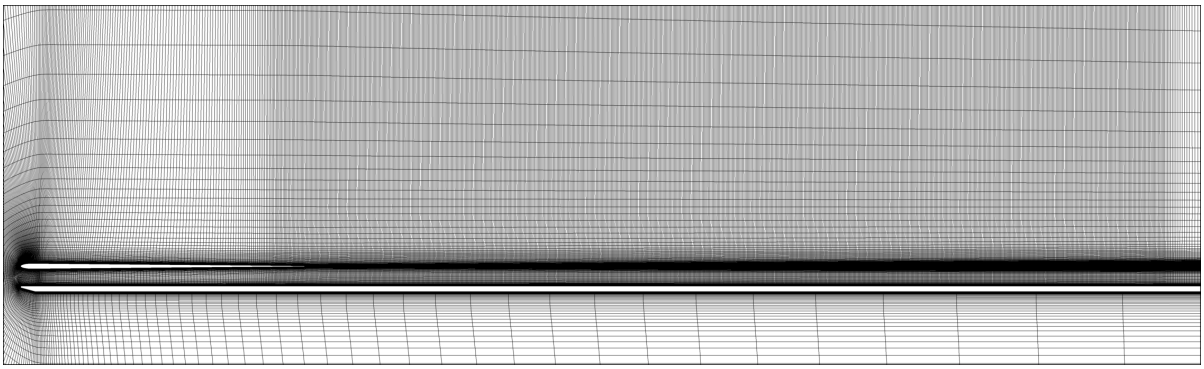

Figure 4: Grid around the flat plates for the co-flow of a wake and a boundary layer

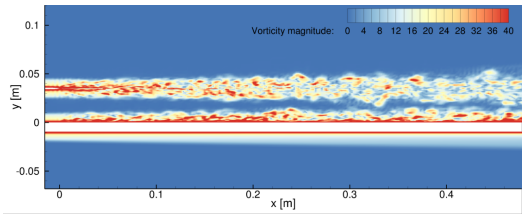

Figure 5: Instantaneous vorticity magnitude for the co-flow in z = constant plane

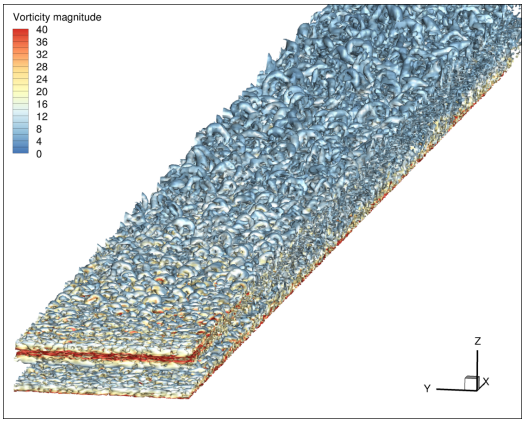

Figure 6: Instantaneous iso-contours of Q criterion for the co-flow in the WMLES region

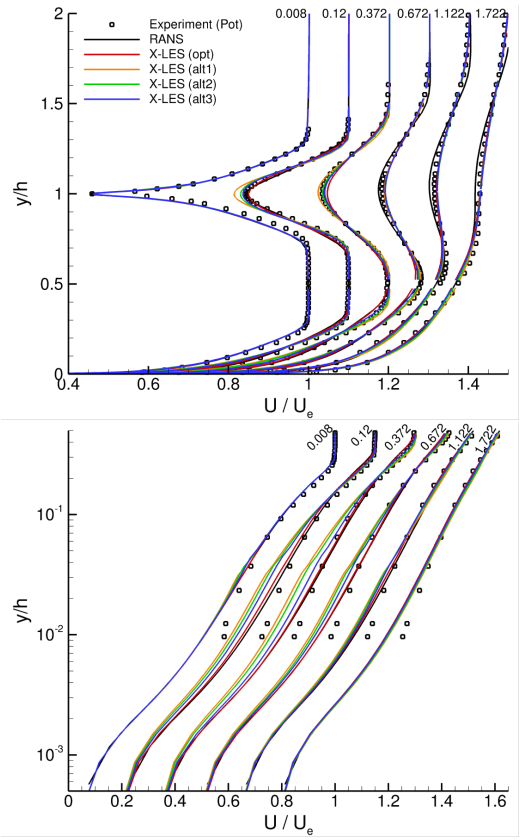

Figure 7: Velocity profiles for the co-flow (additional offset of 0.1 (top) or 0.15 (bottom) for each subsequent section)

(of about 10%) for alternative 1, and the strongest drop (about 20%) for alternative 3. This is in line with the shear stress levels in the first half of the LES target region. The original formulation quickly returns to the RANS levels (within about 0.2 m). The alternatives lag behind until about half the LES target region. In the second half, all WMLES results show a similar gradient, slightly higher than the RANS results. Beyond $x = 1.5$ m, where the modelling gradually returns to RANS, all WMLES results continue at a similar slope as RANS, but the alternative formulation shows a temporary increase (with the strongest increase for alternative 1).

5 Conclusions

The X-LES method has been extended to WMLES mode using a stochastic backscatter model. With optimized values for the model coefficients, the stochastic model practically removes any log layer mismatch between the RANS and LES regions in the velocity profile of a channel flow. For the original stochastic formulation, however, this is partly due to a non-zero mean value of the stochastic source term, which adds an additional, artificial shear stress term to the momentum equations. An alternative formulation of the stochastic model has been proposed that ensures a zero mean value and removes the artificial stress term. For this alternative, three sets of model coefficients have been considered that also essentially remove the log layer mismatch. In terms of the total stresses, the modelling is not entirely seamless at the RANS–LES inter-

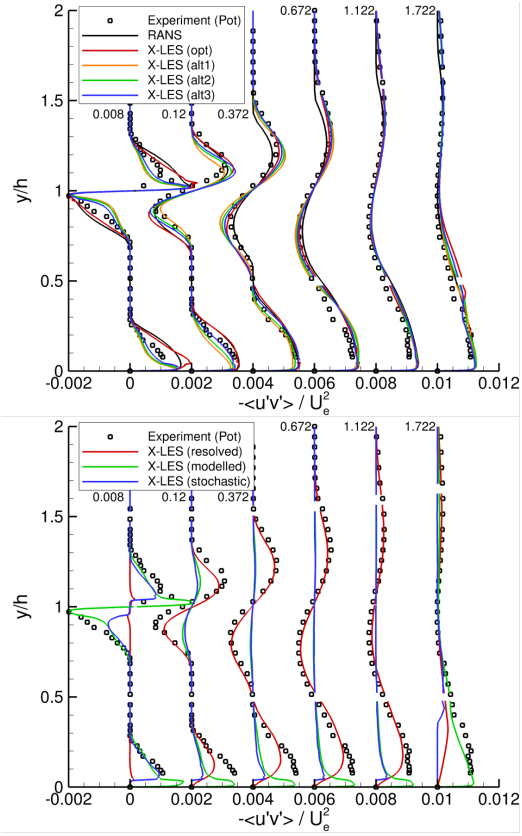

Figure 8: Shear stress profiles for the co-flow (additional offset of 0.002 for each subsequent section; top: total stress; bottom: separate components for original stochastic formulation)

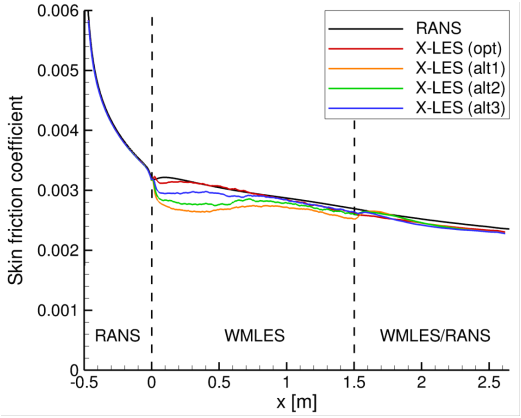

Figure 9: Skin-friction coefficient for the lower plate of the co-flow

face, with a small wiggle remaining in the shear stress and a rapid change of the levels of the normal stresses.

Application to the co-flow of a wake and boundary layer shows that the model also strongly mitigates the grey-area issue both in separated and attached flows. The backscatter model ensures that resolved turbulence rapidly develops after switching from RANS to LES without adding any synthetic turbulence. Especially for the original formulation, the skin friction retains appropriate levels, essentially due to the non-zero mean stochastic term. For the alternative formulation, there is a drop in skin friction levels and the velocity in the inner boundary layer lags behind in the first half of the target LES region. It may be possible to improve the results for the alternative formulation by further optimizing the model coefficients, considering the variation shown between the three different sets of coefficients.

References

Henger, M. (2020), Assessment of the X-LES method and a decomposed turbulence model by application to turbulent channel flow, Master's thesis, Delft University of Technology.

Jarrin, N., Prosser, R., Uribe, J.-C., Benhamadouche, S. and Laurence, D. (2009), 'Reconstruction of turbulent fluctuations for hybrid RANS/LES simulations using a synthetic-eddy method', *International Journal of Heat and Fluid Flow* **30**, 435–442.

Kok, J. C. (2009), 'A high-order low-dispersion symmetry-preserving finite-volume method for compressible flow on curvilinear grids', *Journal of Computational Physics* **228**, 6811–6832. NLR-TP-2008-775.

Kok, J. C. (2017), 'A stochastic backscatter model for grey-area mitigation in detached eddy simulations', *Flow, Turbulence and Combustion* **99**, 119–150. NLR-TP-2016-233.

Kok, J. C., Dol, H. S., Oskam, B. and van der Ven, H. (2004), Extra-large eddy simulation of massively separated flows, *in* '42nd AIAA Aerospace Sciences Meeting', Reno, NV. AIAA paper 2004-264.

Lee, M. and Moser, R. D. (2015), 'Direct numerical simulation of turbulentchannel flow up to $Re_\tau \approx 5200$', *Journal of Fluid Mechanics* **774**, 395–415.

Peng, S.-H., Deck, S., Kok, J. C., Probst, A., Arvidson, S., Moioli, M., Catalano, P., Capizzano, F., Revell, A., Righi, M., Lozano, C., Breitsamter, C. and Tourrette, L. (2020), GARTEUR AG 54 — RaLESin: RANS–LES interface for hybrid RANS–LES and embedded LES, TP 193, GARTEUR.

Piomelli, U., Balaras, E., Pasinato, H., Squires, K. D. and Spalart, P. R. (2003), 'The inner–outer layer interface in large-eddy simulations with wall-layer models', *International Journal of Heat and Fluid Flow* **24**, 538–550.

Pot, P. J. (1979), A wake boundary layer mixing experiment, MP 79012 U, National Aerospace Laboratory NLR, The Netherlands.

Shur, M. L., Spalart, P. R., Strelets, M. K. and Travin, A. K. (2008), 'A hybrid RANS–LES approach with delayed-DES and wall-modelled LES capabilities', *International Journal of Heat and Fluid Flow* **29**, 1638–1649.

Spalart, P. R. (2009), 'Detached-eddy simulation', *Annual Review of Fluid Mechanics* **41**, 181–202.